Voltage Induced Single-Molecule Junction Planarization

Yaping Zang[1‡], E-Dean Fung[1‡], Tianren Fu[2], Suman Ray[3], Marc H. Garner[4], Anders Borges[4], Michael L. Steigerwald[1], Satish Patil[3], Gemma Solomon[4*], Latha Venkataraman[1,2*]

[1]*Department of Applied Physics, Columbia University, New York, NY, U.S.A.*

[2]*Department of Chemistry, Columbia University, New York, NY, U.S.A.*

[3]*Solid State and Structural Chemistry Unit, Indian Institute of Science, Bangalore, India*

[4]*Nano-Science Center and Department of Chemistry, University of Copenhagen, Copenhagen Ø, Denmark*

‡ Equal contribution.

Email: gsolomon@chem.ku.dk, lv2117@columbia.edu

Contents:

1. STM-Break Junction Measurements Methods:

Conductance: Conductance measurements were carried out using a custom scanning tunneling microscope that has been described in detail before.[1] Measurements were made from dilute DPP2 solutions (0.1–1mM) in 1,2,4-trichlorobenzene (TCB) and tetradecane (TD). One-dimensional conductance histograms were constructed using logarithmic bins (100 bins/decade), and two-dimensional histograms used logarithmic bins along the conductance axis (100 bins/decade) and linear bins along the displacement axis (450 bins/nm). All histograms were constructed without any data selection.

Temperature Dependent Measurements: In order to increase the temperature, the STM is modified to include a resistive heating element as described previously [REF]. We use a modified experimental procedure described in the manuscript for these measurements. We first analyze the data by only considering traces that show a molecular plateau with a conductance between 5×10^{-6} G_0 and 10^{-2} G_0 during the first 50 ms region of the hold section. These traces are compiled into 2D conductance-time histograms (Figure S1a-c). We label the traces by comparing the conductance during the first and last hold sections (low-bias). If the conductance is higher during the last hold segment, then the molecular backbone has planarized. We compile traces for junctions that planarize into separate 2D conductance-time histograms (Figure S1d-f), and the fraction of traces that planarize gives us the planarization ratios in Table S1.

Current-Voltage: Current-voltage (I-V) characteristics of DPP2 were determined by carrying out voltage dependent break-junction measurements. For these measurements, a 100kΩ or 1 MΩ resistor was used in series with the junction to prevent the current amplifier from saturating under the high applied bias. All measurements were made using a gain setting of 1V/μA on the current amplifier, except high bias measurements in TD which were made using a gain of 0.1V/μA. A bias ranging from 90 mV to 1.1 V (in ≤ 250 mV increments) was applied to the junction with the resistor in series while forming and breaking the Au point contact in a solution of the molecules. Current through the junction and voltage across the junction were measured as a function of tip/sample displacement. Current and voltage data at each applied voltage were analyzed using log-binned and linearly-binned one-dimensional histograms, respectively. Each data point in Figure 3 (I and V) is extracted from the peak values of current and voltage histograms.

Thermopower: We use a modified experimental procedure that we have described in detail previously in order to determine the thermopower (or Seebeck coefficients) of single-molecule junctions.[2, 3] Briefly, we start with an Au-Au contact and withdraw the tip to form a molecular junction at an applied bias of 10 mV. We then hold the junction for 200 ms before we withdraw the tip further to break the junction. During the central 150 ms of the hold, we set the tip bias to be 0 mV. We collect thousands of such traces with a 0 K, 27 K and 28 K temperature difference between the tip and the substrate.

In order to analyze the data, we only consider traces that show a conductance within the molecular conductance range (as determined from 1D conductance histograms) during the start and end of the hold. For each of these selected traces, the junction thermoelectric current is determined by averaging the measured junction current during the central hold portion (when 0 mV bias is

applied). The thermoelectric current values are then used in conjunction with the average molecular conductance before and after the hold to compute the average Seebeck coefficient of the given molecular junction. Histograms of the measured thermoelectric current and Seebeck coefficient of DPP2 in TCB and TD are shown in Figure S5.

2. DFT Calculations

Transmission calculations.

We use DFT and calculate the transmission functions using the nonequilibrium Green's function (NEGF) formalism as implemented in GPAW and the Atomic Simulation Environment (ASE).[4, 5] We use the projector augmented wave method. The Perdew-Burke-Ernzerhof (PBE) exchange–correlation functional and double-ζ plus polarization basis set was used for the calculations.[6, 7] The DPP2 molecule is simplified by replacing all alkyl chains with ethyl groups due to computational constraints. In order to simulate the metal-molecule-metal system, molecules are optimized in the gas phase and then attached to gold electrodes to form junctions. The electrodes consist of 4×6 fcc Au (111) surfaces with three under-coordinated Au atoms forming a trimer on each surface. The molecule, trimers and top layer of the Au are further relaxed to a maximum atomic force of 0.05 eV $Å^{-1}$ while keeping the remaining Au-atoms fixed. We then calculate the Landauer transmission across these junctions. The Fermi energy is retrieved from the full junction calculation (including Au) using the PBE functional. For the purpose of modelling the effect the solvent has on the Fermi energy, we assumed that the Fermi energy in TCB is that from the junction calculation, and that the Fermi energy in TD is mid-gap as we have illustrated in Figure S6. Finally, we calculate the I-V curves/conductance by numerical integration of the transmission in accordance with the Landauer formula assuming no voltage dependence of the transmission and an electrode temperature of 300K. The I-V curves are shown in Figure 3b in the manuscript.

Rotational barrier calculations.

We first optimized the geometry of DPP2 in its ground state and calculated its electronic structure to obtain isosurface plots of the HOMO and LUMO orbitals using DFT(B3LYP/6-31+G**).[8] To examine the rotational barrier, we take the ground state geometry and rotate the central dihedral angle in steps of 10°. The total energy for the ground, cationic, anionic, and spin-triplet excited state is calculated for each dihedral angle using at the PBE level of theory.[9]

3. Additional Experimental Data and Analysis

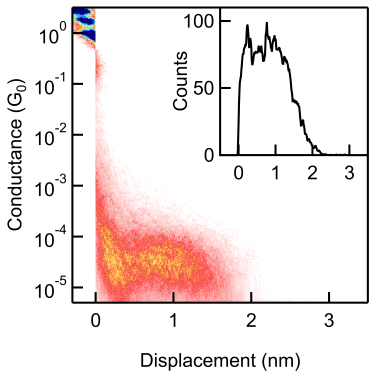

Figure S1. *2D conductance histogram of DPP2 compiled from 1800 traces measured at 0.1 V bias at 289K.*

Temperature-dependent high bias hold data analysis.

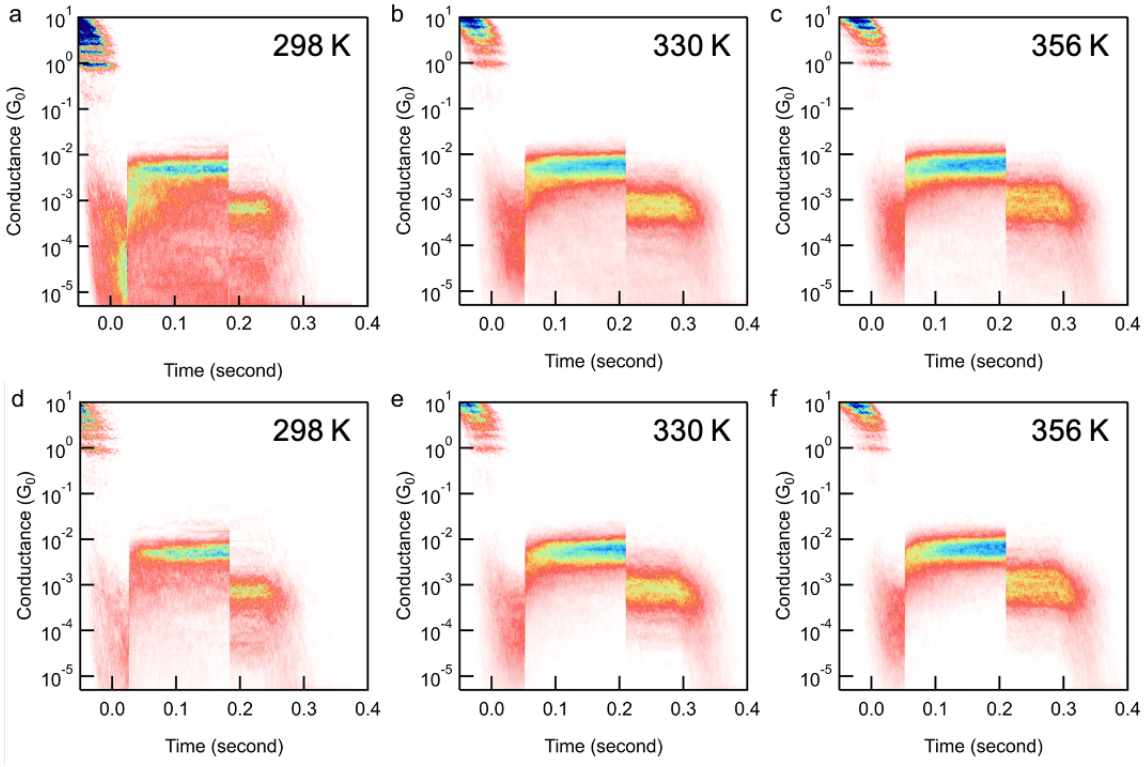

Figure S2. *2D conductance-time histogram of DPP2 compiled from selected traces with a molecular conductance feature acquired at (a) 289 K, (b) 330 K and (c) 356 K. The time axis is relative to the start of the hold section. 2D histogram compiled from selected traces of junction that planarize due to high bias at (d) 289 K (hold segment is 0.2 s), (e) 330 K (hold segment is 0.25 s) and (f) 356 K (hold segment is 0.25 s). These traces are selected following the procedure detailed above and the number of traces selected at each temperature is shown in Table S1.*

Temperature	298 K	330 K	356 K
Selected traces out of 2000	1120	1543	1405
Number of traces that planarize	370	892	888
Fraction of traces that planarize	0.33	0.58	0.63

Table S1. *Temperature dependent measurement results.*

Measurements in TCB

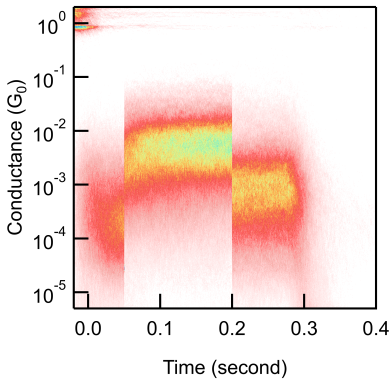

Figure S3. *2D conductance-time histogram of DPP2 compiled from 5000 traces without data selection acquired in TCB. The time axis is relative to the start of the hold section. Hold bias voltage: 0.1 V (0-50 ms, 200-250 ms), 0.75 V (50-200 ms). Although the average conductance is higher in the high bias hold, the variance is comparable in both during and after the high hold, in contrast to what is observed in TD.*

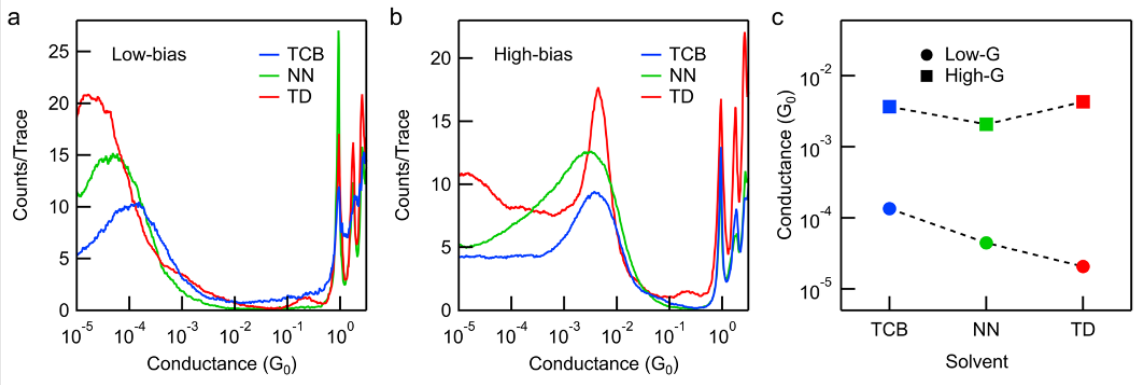

Figure S4. *Logarithm-binned 1D histograms for DPP2 at (a) low and (b) high tip bias in TCB, 1-Nonanol (NN) and TD. The high-bias to achieve resonant transport is 0.75 V in TCB, 0.9 V in NN and 1.4 V in TD. The voltage is applied to the junction with a series resistor of 100 kΩ in TCB and NN and 1 MΩ in TD. (c) The low and high bias conductance determined from Gaussian fits to histogram peaks in (a) and (b). The high-bias conductance is roughly independent of the solvent, whereas the low-bias conductance shows a trend:* $G_{TCB} > G_{NN} > G_{TD}$. *The voltage for achieving resonant transport show the opposite trend, that is* $V_{TCB} < V_{NN} < V_{TD}$. *This indicates that the frontier orbitals shift away from Fermi in TD when compared with NN and TCB. We also note that in TD, the high-bias conductance peak width is much smaller than in both TCB and NN(b).*

Bias Dependent Measurements.

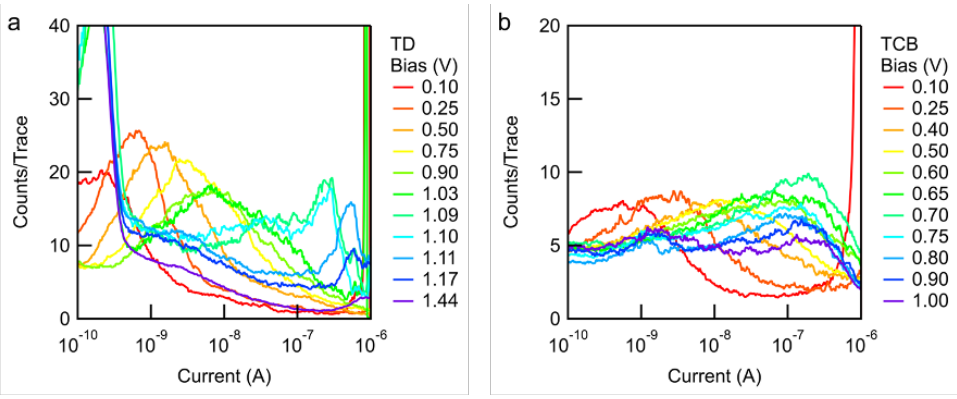

Figure S5. *Current histograms measured with DPP2 using (a) TD as solvent and (b) TCB as solvent. All measurements in TCB performed with 100 kΩ resistor and 1 V/μA gain. Measurements in TD with bias greater than 1 V performed with MΩ resistor and 0.1 V/μA gain. The peak above* 10^{-10} *Amps at higher bias corresponds to the instrument noise at higher gain.*

Thermopower Measurements.

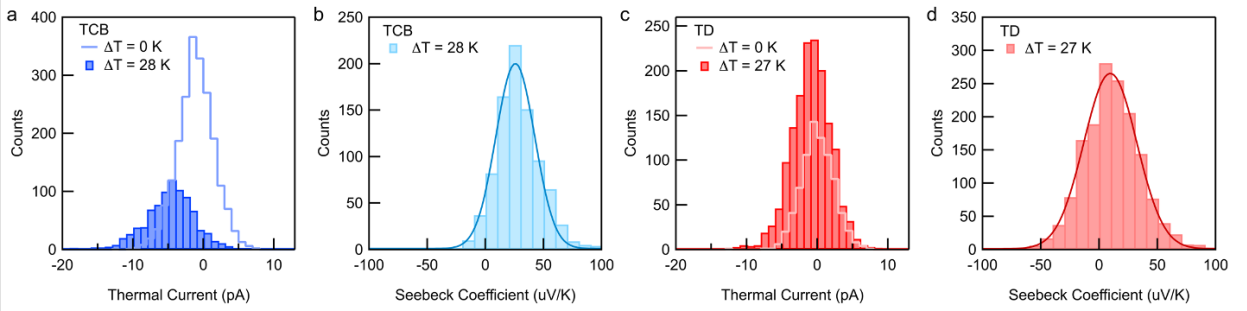

Figure S6. *(a, c) Thermoelectric current and (b, d) Seebeck coefficient histograms for DPP2 in TCB (a, b) and TD (c, d). At ΔT=0 K, the thermoelectric current peak is at 0 pA for both TCB and TD measurements, indicating there is no current flowing without a temperature gradient (and a bias voltage) applied. At a ΔT of 28K, for the TCB measurements, the thermoelectric current shifts to a negative value and we get a positive Seebeck coefficient of 26 μV/K, indicating HOMO is the orbital which is aligned closest to the Fermi level. In TD, at a ΔT of 27K, we find a smaller thermoelectric current (close to 0 pA) and a Seebeck coefficient of 9.6 μV/K, indicating that the orbital alignment is closer to mid-gap. These results demonstrate the shift of molecular resonances relative to Fermi due to solvent-induced static gating effect and account for the proposed one-channel (in TCB) and two-channel (in TD) resonant transport model in Figure 3.*

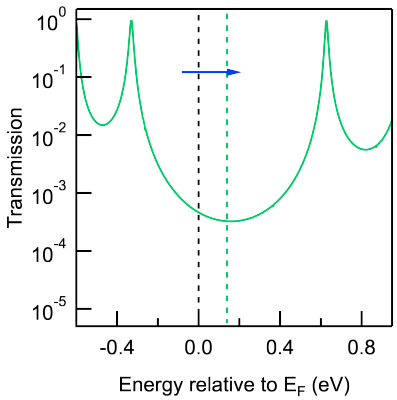

Figure S7. *DFT-based transmission as a function of energy for DPP2. We use the HOMO and LUMO positions relative to the Fermi level to model the one-channel transport in TCB. We offset the E_F by 0.14 eV to model the mid-gap alignment in TD. We calculated the I-V and dI/dV curves for these two different alignments based on Landauer formula.*

4. References

(1) Venkataraman, L.; Klare, J. E.; Tam, I. W.; Nuckolls, C.; Hybertsen, M. S.; Steigerwald, M. L., Single-molecule circuits with well-defined molecular conductance, *Nano Lett.,* **2006,** 6, 458-62.

(2) Dell, E. J.; Capozzi, B.; Xia, J.; Venkataraman, L.; Campos, L. M., Molecular length dictates the nature of charge carriers in single-molecule junctions of oxidized oligothiophenes, *Nat. Chem.,* **2015,** 7, 209-14.

(3) Widawsky, J. R.; Darancet, P.; Neaton, J. B.; Venkataraman, L., Simultaneous determination of conductance and thermopower of single molecule junctions, *Nano Lett.,* **2012,** 12, 354-8.

(4) Hjorth Larsen, A., et al., The atomic simulation environment-a Python library for working with atoms, *J. Phys.: Condens. Matter,* **2017,** 29, 273002.

(5) Mortensen, J. J.; Hansen, L. B.; Jacobsen, K. W., Real-space grid implementation of the projector augmented wave method, *Phys. Rev. B,* **2005,** 71.

(6) Larsen, A. H.; Vanin, M.; Mortensen, J. J.; Thygesen, K. S.; Jacobsen, K. W., Localized atomic basis set in the projector augmented wave method, *Phys. Rev. B,* **2009,** 80.

(7) Perdew, J. P.; Burke, K.; Ernzerhof, M., Generalized Gradient Approximation Made Simple, *Phys. Rev. Lett.,* **1996,** 77, 3865-3868.

(8) Bochevarov, A. D., et al., Jaguar: A high-performance quantum chemistry software program with strengths in life and materials sciences, *Int. J. Quant. Chem.,* **2013,** 113, 2110-2142.

(9) Havu, V.; Blum, V.; Havu, P.; Scheffler, M., Efficient integration for all-electron electronic structure calculation using numeric basis functions, *J. Comp. Phys.,* **2009,** 228, 8367-8379.